Development of Fine Pointing Mechanism for Optical Inter-Satellite Communication

Seiichi Shimizu, Kazuhiko Fukushima,
Kazuhide Kodeki
Mitsubishi Electric Corporation
Advanced Technology R&D Center
8-1-1 Tsukaguchihonmachi, Amagasaki, Hyougo 661-8661, Japan
Shimizu.Seiichi@ct.MitsubishiElectric.co.jp

Toshiyuki Ando
Mitsubishi Electric Corporation
Information Technology R&D Center
5-1-1 Ofuna, Kamakura, Kanagawa 247-8501, Japan
Tomohiro Araki
Japan Aerospace Exploration Agency
Aerospace Research and Development Directorate
2-1-1 Sengen, Tsukuba, Ibaraki 305-8505, Japan

***Abstract*— Laser-based optical inter-satellite communication equipment permits large-capacity communication, which is essential for future observation satellites that will handle huge amounts of data. Among the key technologies for optical inter-satellite communication equipment are rapid, highly accurate acquisition and tracking technologies for the corresponding satellites. Therefore, the Mitsubishi Electric Corporation and the Japan Aerospace Exploration Agency are developing a fine pointing mechanism for optical inter-satellite communication. The fine pointing mechanism is designed to be installed in a geostationary satellite, and the design life of the fine pointing mechanism is 15 years. This paper describes the specifications, mechanism, control system, and performance evaluation results of the fine pointing mechanism.**

Keywords*— *Optical inter-satellite communication, Optical antenna, Acquisition and tracking system, Fine pointing mechanism

I. Introduction

The emerging development of observation and other low-Earth-orbit (LEO) satellites capable of greatly expanded high-volume data acquisition is expected to increase the need for high-speed data transmission. This need is compounded by the limited time window available for direct communication between a LEO satellite and a ground-based antenna and the resulting requirement for high-volume data transmission. In addition, the size of the radio-frequency communication terminal must increase as the transmission speed increases. We are therefore engaged in the investigation and development of small, lightweight optical communication components that will permit high-speed communication by a laser beam between a LEO satellite and a data relay satellite in the geostationary Earth orbit (GEO) (Fig. 1).

Because optical inter-satellite communication can transmit a beam whose power is concentrated by an optical antenna with high directivity, small size and lightweight communication equipment and large-capacity communication become feasible. However, because of the high directivity of the laser beam, optical inter-satellite communication requires a pointing accuracy that is 1 or 2 digits higher than that obtained through communication by radio waves.

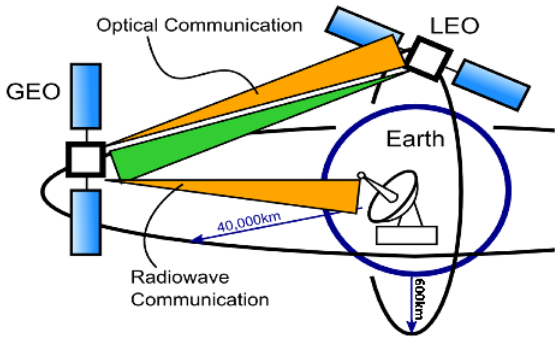

Fig. 1. Laser communication between low-Earth-orbit (LEO) satellite and geostationary-Earth-orbit (GEO) satellite.

Therefore, for optical inter-satellite communication, high-speed transmission technology and highly accurate (several microradians) acquisition and tracking technology for the corresponding satellite are key technologies, and some elements of this optical communication equipment have been manufactured.

The design life of the optical communication equipment in orbit is 15 years, which is the same as the design life of a GEO satellite. It is essential that optical communication equipment have sufficiently high reliability to perform over this design life.

The acquisition and tracking system consists of pointing sensors—a coarse pointing sensor (CPS) for initial acquisition and a fine pointing sensor (FPS) for tracking—which detect the pointing angle error based on the arrival direction of the received beam; a coarse pointing mechanism (CPM), which corrects the pointing angle error automatically; a fine pointing mechanism (FPM); and a point-ahead mechanism (PAM), which corrects the aberration of the beam from the corresponding satellite.

Characteristic features of the prototype FPM that we have developed are its frictionless rotational mechanism, its wide driving range, its wide control bandwidth, its high control accuracy, and its low power consumption. Additionally, the FPM was designed with the severe environment associated with launching taken into consideration.

In this paper, the specifications and configuration of the FPM are described, and the results of an environmental test and performance evaluation are described.

II. Outline of FPM

Key properties of the prototype FPM are listed in Table 1, and photographs of the prototype FPM are shown in Figures 2 and 3. The inner moving part of the FPM and the holding part of the FPM are connected by two flexural pivots. Two additional flexural pivots connect the inner moving part and outer moving part of the FPM. Because the flexural pivots have a contactless rotational hinge structure, the FPM has a frictionless rotational mechanism. Either voice coil actuators or electromagnetic actuators can be used as with the FPM. The driving force of a voice coil actuator is proportional to the current. On the other hand, the driving force of an electromagnetic actuator is proportional to the square of the current. An electromagnetic actuator has higher drive efficiency than a voice coil actuator of the same size. In addition, because an electromagnetic actuator has no magnet, it has a robust mechanism. It is a problem that electromagnetic actuators have nonlinear characteristics, but the control program can compensate for these. Four electromagnetic actuators are used in the prototype FPM to control the moving part. The use of electromagnetic actuators reduces the amount of power consumed by the FPM (to a maximum of 1.3 W) and reduces the amount of heat generated. In addition, the use of silicon steel for the electromagnetic actuators reduces the outbreak of the eddy current and achieves high-speed drive. The design and trial manufacture of the FPM was accomplished completed using parts for which the demand lifetime is guaranteed. The lifetime evaluation method of the moving part of the FPM was examined, but this topic is not addressed in this paper here. Figure 4 shows the examination details for the FPM.

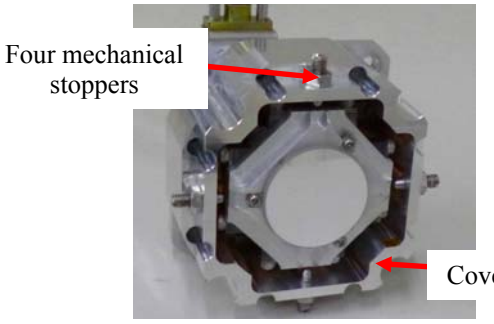

Fig. 2. Prototype of FPM (with cover).

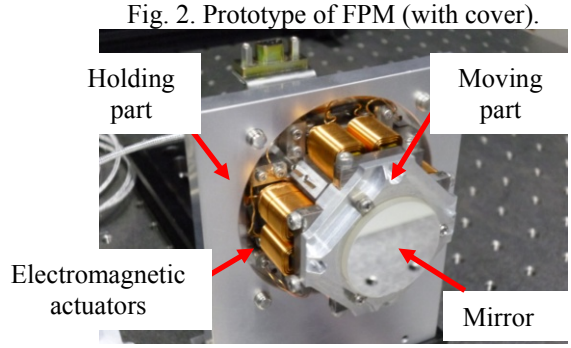

Fig. 3. Prototype of FPM (without cover).

Table 1. Key properties of prototype FPM

Parameter	Specification
Driving range	(High-accuracy control): more than ±0.5° (Wide-angle driving): more than ±2°
Control accuracy	(High-accuracy control): within 20 μrad (Wide-angle driving): within 100 μrad
Control bandwidth	(High-accuracy control): more than 300 Hz; 600 Hz desired (Wide-angle driving): more than 30 Hz
Lifetime	Orbital lifetime: 15 years (Operation duty 65%)
Environmental resistance	Random vibration level: 20 Grms Shock level: 1,000 Gsrs
Mirror diameter	φ: 30 mm
Wavelength	1–1.6 μm
Actuator	Electromagnetic type
Local sensor	Capacitive sensor
Size	66×66×50 mm (without launch lock mechanism)
Weight	0.3 kg (without launch lock mechanism)
Power consumption	Maximum of 1.3 W

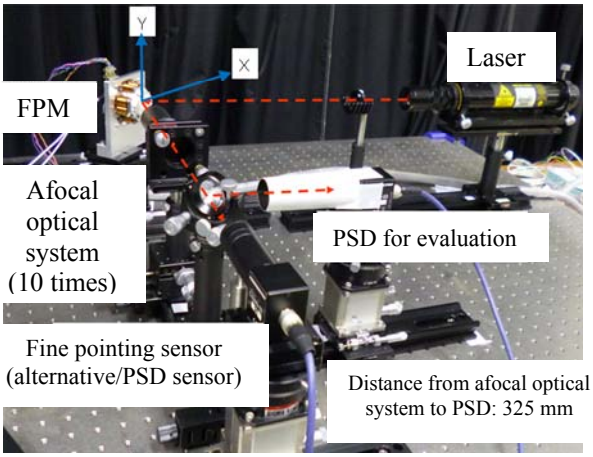

Fig. 4. Examination situation of FPM.

III. Control Design of FPM

Figure 5 shows a control system block diagram for the FPM. The FPM suppresses vibration transmitted to the sensors from the satellite and the disturbance of the CPM, and the communication beam from the corresponding satellite is focused near the origin of the FPS. Therefore, the proportional-integral-derivative (PID) control law applies to the FPM. In addition, the nonlinearity of the electromagnetic actuator is proportional to the square of the current and inversely proportional to the square of the gap and can be a factor in control performance deterioration. Therefore, linearization of the actuator is accomplished by calculating the size of the actuator gap and correcting the gap based on the tilting angle from a local sensor and by adding a bias current to the control current.

IV. Performance Evaluation

Figures 6–9 show measurement results obtained for the driving range of the FPM. The driving range can be achieved with a specification machine angle of more than ±1° (an optical axis conversion angle of ±2°). During initial capture, or when the communication beam does not come from the corresponding satellite, the FPM is controlled using the local sensor. Figures 10 and 11 show the open-loop transfer-function frequency characteristics of the FPM control system in the case of control by the local sensor. The control bandwidth of the FPM is 144.9 Hz for rotation in the X-axis direction and 145.4 Hz for rotation in the Y-axis direction. Both of these measured values exceed the specified minimum value of 30 Hz.

Figures 12 and 13 show the tracking accuracy time response characteristics of the FPM control system in the case of control by the local sensor. The tracking accuracy is 53.3 μrad (3σ) for rotation in the X-axis direction and 72.2 μrad (3σ) for rotation in the Y-axis direction. Both of these measured values exceed the specified range of 100 μrad (3σ).

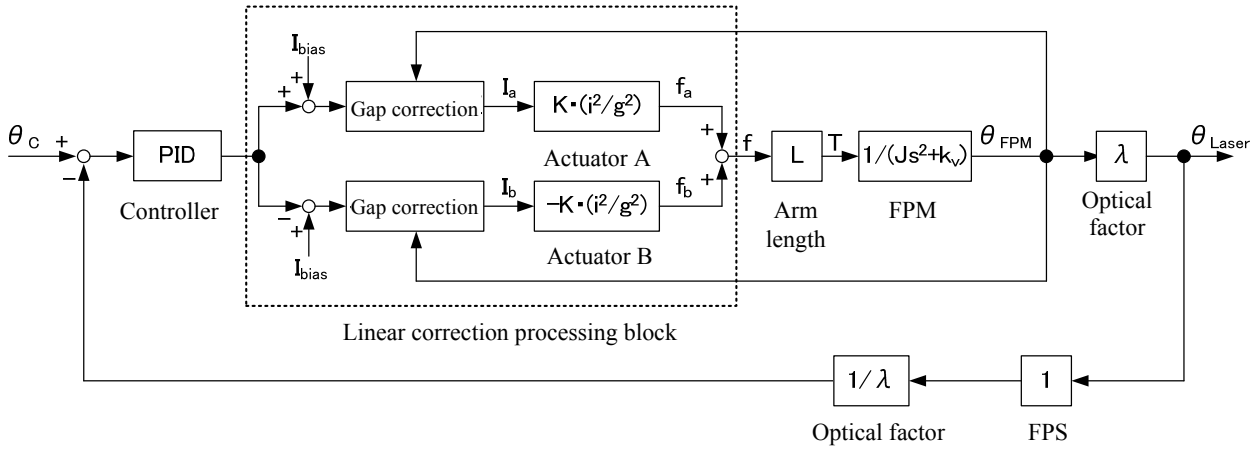

Fig. 5. Control system block diagram of FPM.

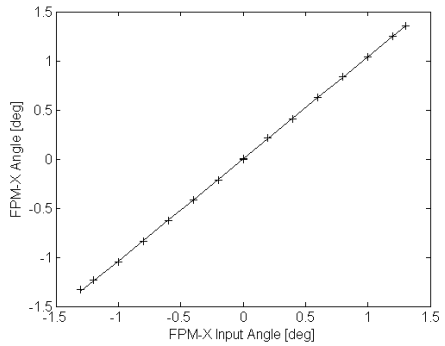

Fig. 6. Driving range in X-axis rotation direction (driving in X-axis rotation direction).

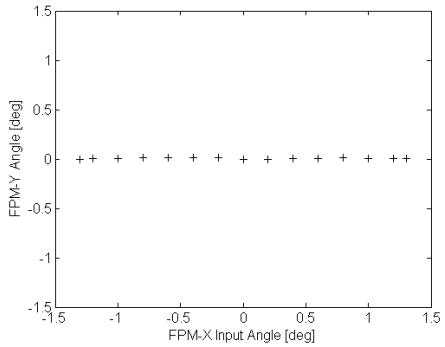

Fig. 7. Driving range in Y-axis rotation direction (driving in X-axis rotation direction).

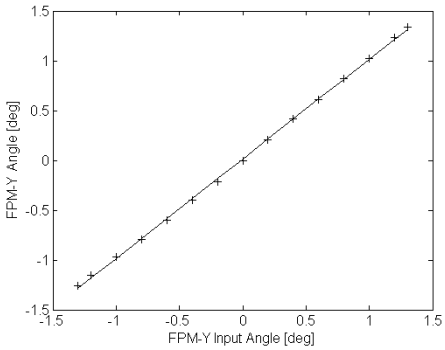

Fig. 8. Driving range in Y-axis rotation direction (driving in Y-axis rotation direction).

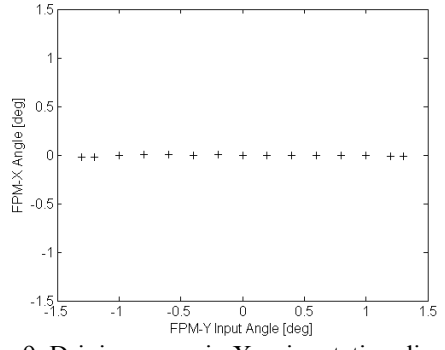

Fig. 9. Driving range in X-axis rotation direction (driving in Y-axis rotation direction).

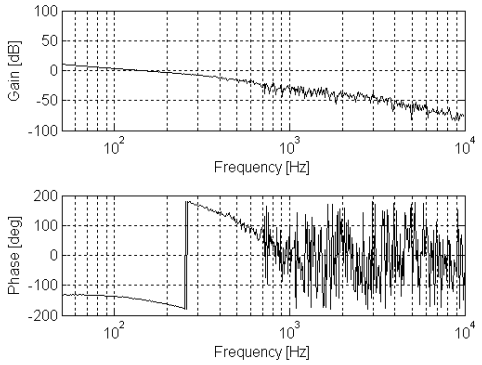

Fig. 10. Control bandwidth in X-axis rotation direction (open-loop transfer-function frequency characteristics).

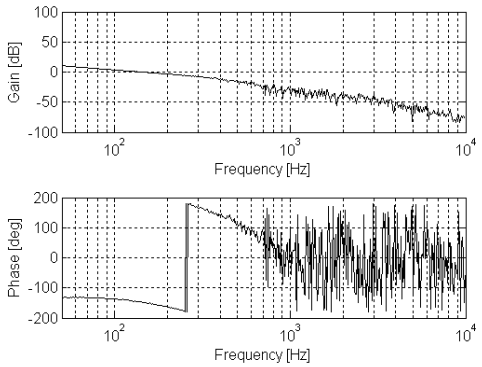

Fig. 11. Control bandwidth in Y-axis rotation direction (open-loop transfer-function frequency characteristics).

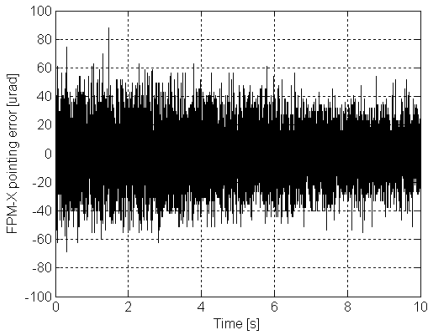

Fig. 12. Control accuracy in X-axis rotation direction (optical axis conversion angle).

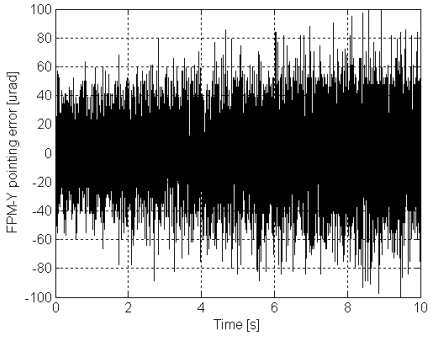

Fig. 13. Control accuracy in Y-axis rotation direction (optical axis conversion angle).

During tracking or communication, the FPM is controlled using the FPS. Figures 14 and 15 show the open-loop transfer-function frequency characteristics of the FPM control system in the case of control by the FPS. The control bandwidth of the FPM is 316.0 Hz for rotation in the X-axis direction and 318.5 Hz for rotation in the Y-axis direction. Both of these measured values exceed the specified minimum value of 300 Hz.

Figures 16 and 17 show the tracking accuracy time response characteristics of the FPM control system in the case of control by the PSD sensor, which is an alternative to the FPS. The tracking accuracy is 3.9 μrad (3σ) for rotation in the X-axis direction and 7.1 μrad (3σ) for rotation in the Y-axis rotation. Both of these measured values are within the specified range of 20 μrad (3σ).

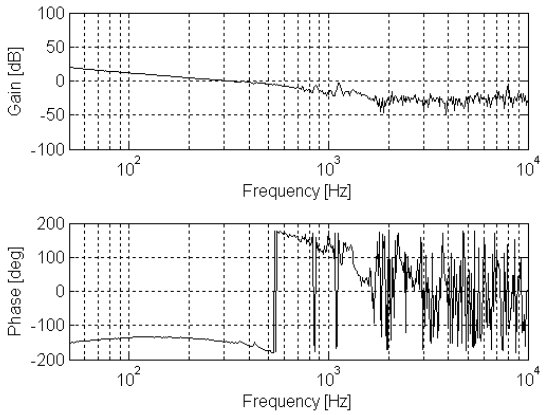

Fig. 14. Control bandwidth in X-axis rotation direction (open-loop transfer-function frequency characteristics).

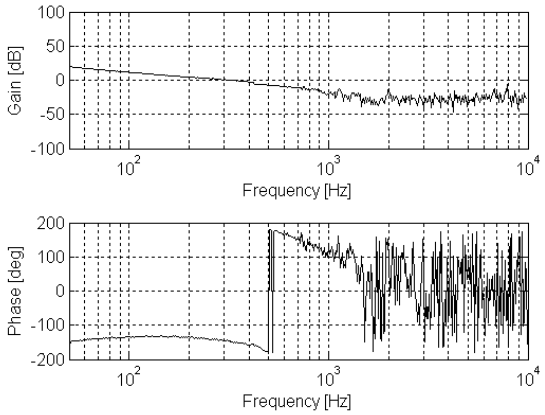

Fig. 15. Control bandwidth in Y-axis rotation direction (open-loop transfer-function frequency characteristics).

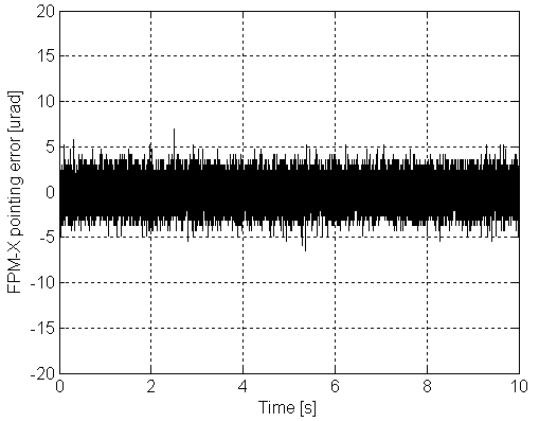

Fig. 16. Control accuracy in X-axis rotation direction (optical axis conversion angle).

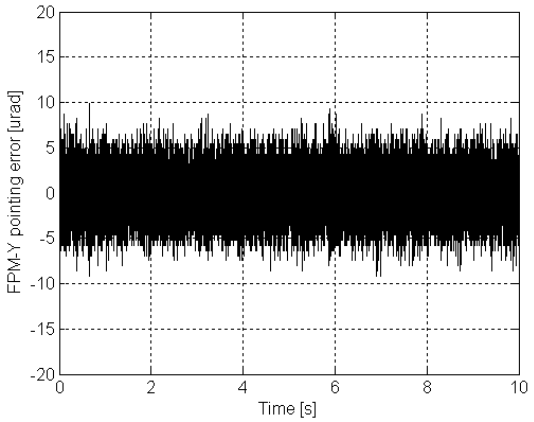

Fig. 17. Control accuracy in Y-axis rotation direction (optical axis conversion angle).

v. Environmental Tests

The main mechanical elements of the FPM are flexural pivots and electromagnetic actuators. Because the flexural pivots are made of steel and the actuators consist of only iron cores and coils, they are not influenced by radiation. Additionally, all of the elements of the pivots and actuators are usable over a wide temperature range and do not possess any parts that are critical with respect to heat. Vibration and shock resistance must be considered in the design of the elements of the flexural pivots, which have a rotational plate spring structure. Therefore, mechanical environmental tests of the FPM were carried out. A vibration test of the FPM was carried out under the sine-wave sweep conditions summarized in Table 2 for the random vibration profile shown in Figure 18. Figure 19 shows the vibration test conditions for the FPM.

Figure 20 shows an example of the shock test profile. The shock test was carried out at a shock level of 450 Gsrs. A test at a shock level of 1,000 Gsrs will be carried out in the future. Figure 21 shows the conditions of the shock test. The results of a performance evaluation conducted after the vibration and shock tests confirmed that there was no difference in the performance of the FPM before and after the environmental tests and that the FPM maintained its soundness.

Table 2. Sine-wave sweep

Frequency [Hz]	Accelerator or magnitude	Sweep rate [oct/min]
5–19.94	Mag. 12.5 [mm]	2
19.94–100	Acc. 20 G	2

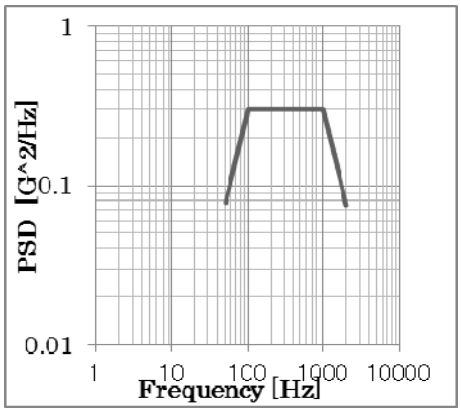

Frequency	PSD
50	0.075
70	0.147
100	0.3
1000	0.3
1500	0.133
2000	0.075
O.A.	20.71 Grms

Vibration time: 180 s

Fig. 18. Random vibration.

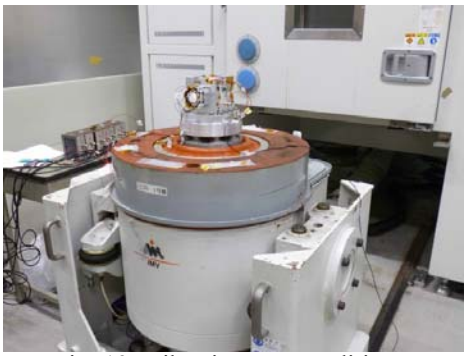

Fig. 19. Vibration test conditions.

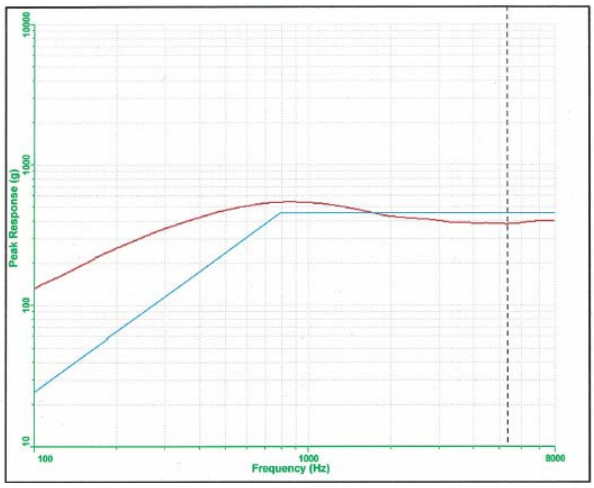

Fig. 20. Shock test profile (SRS).

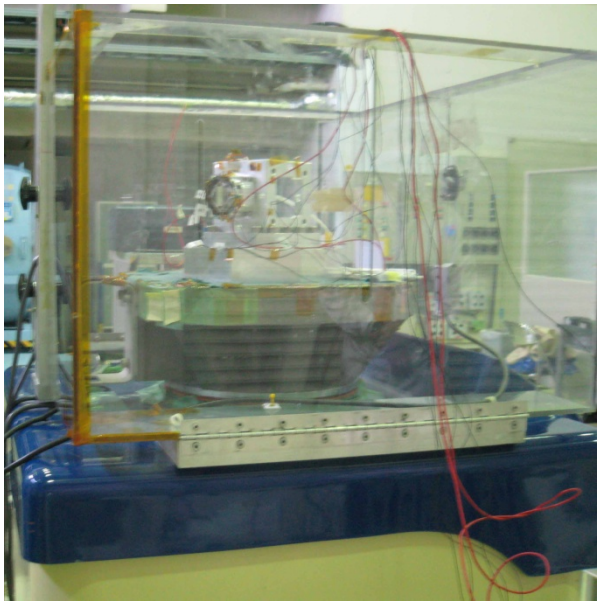

Fig. 21. Shock test conditions.

VI. Conclusions

Details of the specifications, configuration, and performance evaluation results for the prototype FPM for inter-satellite communication under development are described in this paper. Experimental tests verified that the control performance meets the demand specifications for the FPM control system, using either the local sensor or the PSD sensor, as an alternative to the FPS. In addition, environmental tests were carried out, and it was verified that the control performance of the FPM did not change after being subjected to the shock and vibration conditions of the tests.

References

[1] Tomohiro Araki, "The Approach to Realize a Higher Speed, More Compact and Longer-Lasting Operational Optical Space Communications System," ICSOS2014, 2014.

[2] Toshiyuki Ando, Eisuke Haraguchi, Takashi Sugihara, Jiro Suzuki, Kazuhide Kodeki, Tomohiro Araki, "Dual Wavelength Optical Coherent Receiver Front End for Inter-Satellite Communication," ICSOS2014, 2014.

[3] Yoshikuni Miyata, Kenya Sugihara, Wataru Matsumoto, Toshiyuki Ando, "High Reliable Optical Satellite Communications Using an Network Coding," ICSOS2014, 2014.